Nuclear Instruments and Methods in Physics Research A 604 (2009) 512–526

Contents lists available at ScienceDirect

Nuclear Instruments and Methods in Physics Research A

journal homepage: www.elsevier.com/locate/nima

# New crystals for dual-readout calorimetry

N. Akchurin [a], F. Bedeschi [b], A. Cardini [c], R. Carosi [b], G. Ciapetti [d], R. Ferrari [e], S. Franchino [f], M. Fraternali [f], G. Gaudio [e], J. Hauptman [g], M. Incagli [b], M. Korzhik [h], F. Lacava [d], L. La Rotonda [i], M. Livan [f], E. Meoni [i], M. Nikl [j], D. Pinci [d], A. Policicchio [i,1], S. Popescu [a], F. Scuri [b], A. Sill [a], W. Vandelli [k], A. Vedda [l], T. Venturelli [i], C. Voena [d], I. Volobouev [a], R. Wigmans [a,*]

[a] Texas Tech University, Lubbock, TX, USA
[b] Dipartimento di Fisica, Università di Pisa and INFN Sezione di Pisa, Italy
[c] Dipartimento di Fisica, Università di Cagliari and INFN Sezione di Cagliari, Italy
[d] Dipartimento di Fisica, Università di Roma "La Sapienza" and INFN Sezione di Roma, Italy
[e] INFN Sezione di Pavia, Italy
[f] INFN Sezione di Pavia and Dipartimento di Fisica Nucleare e Teorica, Università di Pavia, Italy
[g] Iowa State University, Ames, IA, USA
[h] Institute for Nuclear Problems, Minsk, Belarus
[i] Dipartimento di Fisica, Università della Calabria and INFN Cosenza, Italy
[j] Institute of Physics, Prague, Czech Republic
[k] CERN, Genève, Switzerland
[l] INFM and Department of Materials Science, Università di Milano-Bicocca, Italy

ARTICLE INFO

*Article history:*
Received 19 January 2009
Received in revised form
26 February 2009
Accepted 5 March 2009
Available online 5 April 2009

*Keywords:*
Calorimetry
Cherenkov light
High-$Z$ scintillating crystals

ABSTRACT

Lead tungstate crystals doped with small fractions of praesodynium or molybdenum have been tested in beams of high-energy electrons. The goal of these tests was to study the effects of such dopants on the capability to separate the signal components deriving from the Cherenkov and scintillation light generated by the beam particles. These studies were carried out in view of the possible application of such crystals in dual-readout calorimeters.



## 1. Introduction

It is a well-known fact that homogeneous calorimeters, such as those consisting of scintillating crystals, while being excellent detectors of particles developing electromagnetic (em) showers, deliver very poor performance when it comes to detecting hadrons and jets [1]. This is a direct result of their very large $e/h$ ratio, e.g., 2.4 for high-$Z$ crystals such as lead tungstate ($PbWO_4$). However, recently interest in using such crystals for the electromagnetic section of a general-purpose calorimeter system has revived because of the potential possibility to separate the signals from such crystals into components deriving from Cherenkov light and scintillation light. This would open the way to use such crystals as *dual-readout calorimeters*. Event-by-event measurements of the em fraction of showers induced by hadrons or jets, which is possible in such calorimeters, eliminates the main reason for the poor hadronic performance.

In a recent paper [2], we have demonstrated that a significant fraction of the signals from scintillating lead tungstate ($PbWO_4$) crystals is due to Cherenkov radiation. This was concluded from measurements of the time structure of the signals and from the non-isotropic nature of the light generated by high-energy electrons and muons traversing a $PbWO_4$ crystal. The measurements showed that Cherenkov light contributed, on average, up to 15% to the signals generated by these particles in the crystal used for these studies, at room temperature.

In a follow-up study, we determined the precision with which the contribution of Cherenkov light to the $PbWO_4$ signals could be determined event by event [3]. It turned out that a good separation of the scintillation and Cherenkov components required both a detailed measurement of the time structure of the signals and directional information on the produced light. The latter information is usually not available in the hermetic $4\pi$ detectors that characterize modern particle physics experiments. On the basis of time structure information alone, the measurement precision of

* Corresponding author. Fax: +1 806 742 1182.
*E-mail address:* wigmans@ttu.edu (R. Wigmans).
[1] Now at Department of Physics, University of Washington, Seattle, WA, USA.

0168-9002/$ - see front matter © 2009 Elsevier B.V. All rights reserved.
doi:10.1016/j.nima.2009.03.101

the Cherenkov fraction was found to be limited to ~8%, mainly as a consequence of the fact that the scintillation process in $PbWO_4$ is very fast (decay time ~10 ns, depending on the temperature [4]), and thus hard to distinguish from the prompt production of Cherenkov light.

Better results were obtained with a BGO crystal [3]. This is a much brighter scintillator than $PbWO_4$ and, therefore, Cherenkov light only represents a small fraction of 1% of the light produced in this material by relativistic ionizing particles. However, since the spectra of the two types of light are very different, we managed to obtain an excellent separation by filtering the light. In addition, the relatively long decay time of the scintillation component (300 ns) was helpful in separating it from the prompt Cherenkov component.

Based on this experience, we decided to explore the possibility to combine these advantages of BGO with the intrinsically much higher Cherenkov fraction of $PbWO_4$. To this end, we developed a number of dedicated $PbWO_4$ crystals doped with small fractions of impurities chosen such as to achieve a shift of the scintillation spectrum to longer wavelengths, and a longer decay time.

In Section 2, these crystals and the experimental setup in which they were tested are described, as well as the calibration and data analysis methods that were used. Experimental results are presented in Section 3. In Section 4, we discuss the implications of these results. Conclusions are presented in Section 5.

## 2. Equipment and measurements

### 2.1. Detectors and beam line

The measurements described in this paper were performed in the H4 beam line of the Super Proton Synchrotron at CERN. Our detector was a high-density crystal. Two different types of crystals were studied in these tests:

(1) $PbWO_4$ crystals doped with molybdenum (Mo). The Mo concentration was 1% in one crystal, 5% in the other. The molybdenum impurity substitutes the tungsten ion in the matrix and forms a $MoO_4$ complex, which has a large cross-section for electron capture, and acts as a wavelength shifter. The effect of this is illustrated in Fig. 1, which shows the radioluminescence spectra measured on small samples of doped and undoped $PbWO_4$ [5]. The maximum of the emission is shifted from ~420 to ~510 nm. There is very little difference between the effects of the 1% and 5% Mo concentration in this measurement.

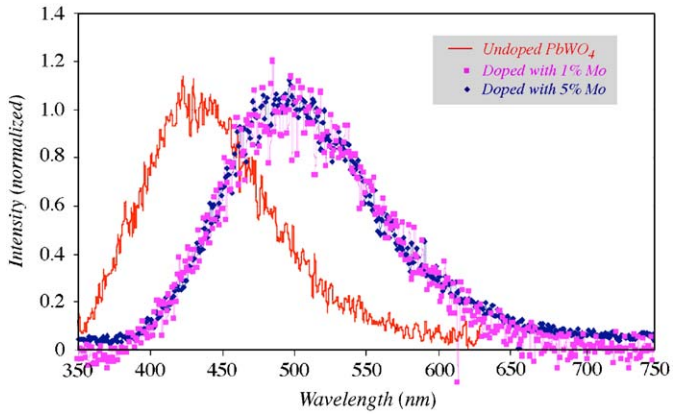


**Fig. 1.** Radioluminescence spectra of small undoped (red) and Mo-doped lead tungstate samples, measured at room temperature [5]. (For interpretation of the references to colour in this figure legend, the reader is referred to the web version of this article.)

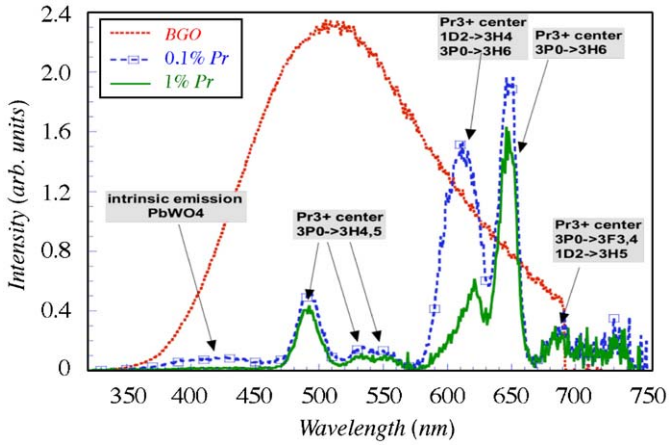


**Fig. 2.** Radioluminescence spectra of small lead tungstate samples, doped with 0.1% or 1% of praesodynium. The spectrum of a BGO crystal is shown for comparison [6].

(2) $PbWO_4$ crystals doped with praesodynium (Pr). The Pr concentration was 0.5%, 1%, 1.5% in the three crystals treated this way. The $Pr^{+3}$ dopant quenches the intrinsic scintillation in the host crystal.
On the other hand, it introduces new scintillation components with long time constants (in the μs range), based on $Pr^{3+}$ 4f–4f transitions in the green–red part of the spectra. This is illustrated in Fig. 2, which shows radioluminescence spectra of small $PbWO_4$ doped with 0.1% or 1% Pr. The emission spectrum of BGO, which peaks at 480 nm, is shown for comparison [6].

An undoped crystal from the same production batch was used for reference purposes. All crystals were produced by the Radiation Instruments & New Components company in Minsk (Belarus). They had a length of 20 cm and a cross-section of $2.0 \times 2.0\,cm^2$. The transverse dimension, relevant for our measurements, corresponded to 2.25 radiation lengths ($X_0$). The light produced by particles traversing this crystal was read out by two photomultiplier tubes (PMTs) located at opposite ends. We used two types of Hamamatsu R5900U tubes for this purpose. Both types had 10 multiplication stages and were equipped with a borosilicate window. One type, to be called $PMT_S$ (standard), had a bi-alkali photocathode, the other type, to be called $PMT_R$ (red extended) had a multi-alkali photocathode. The latter substantially increased the quantum efficiency for longer-wavelength light.

The application of these different PMTs depended on the type of filter that was used to select the wavelength region that contributed to the signal. Table 1 lists the properties of the different optical transmission filters that were used in our studies. Photomultiplier $PMT_S$ was primarily used in conjunction with a high-pass filter[2] (UV or blue), whereas $PMT_R$ was used with a low-pass filter (yellow, orange or red). In order to reduce the light trapping effects of the large refractive index of $PbWO_4$ ($n = 2.2$), the PMTs were coupled to the crystal by means of silicone "cookies" ($n = 1.403$).

The crystal under study was mounted on a platform that could rotate around a vertical axis. The crystal was oriented in the horizontal plane and the rotation axis went through its

[2] The terms high-pass and low-pass refer to the frequency of the light waves, as in electronics applications.

**Table 1**
Properties of the different optical transmission filters that were used in the studies of the doped $PbWO_4$ crystals.

| Filter type | Filter name | >90% transmission for |
|---|---|---|
| UG11 | UV | $\lambda < 400$ nm |
| BG3 | Blue | $\lambda < 500$ nm |
| GG495 | Yellow | $\lambda > 495$ nm |
| OG570 | Orange | $\lambda > 570$ nm |
| RG610 | Red | $\lambda > 610$ nm |

All filters were 3 mm thick, made of glass and produced by Schott.

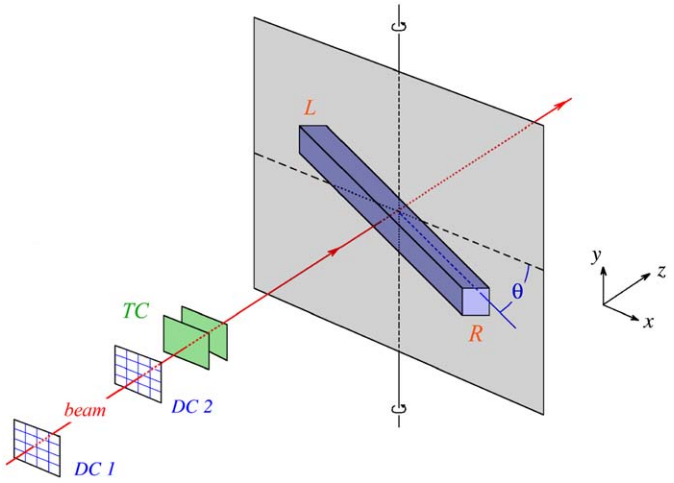


**Fig. 3.** Experimental setup in which the beam tests of the crystals were performed. The angle $\theta$ is negative when the crystal is oriented as drawn here.

geometrical center. The particle beam was also steered through this center, as illustrated in Fig. 3. The angle $\theta$, which is frequently used in the following, represents the angle between the crystal axis and a plane perpendicular to the beam line. The angle increases when the crystal is rotated such that the crystal axis $L$–$R$ approaches the direction of the traveling beam particles. The crystal orientation shown in Fig. 3 corresponds to $\theta = -30^\circ$.

Two small scintillation counters (TC) provided the signals that were used to trigger the data acquisition system. These trigger counters were 2.5 mm thick, and the area of overlap was $6 \times 6\,\text{cm}^2$. A coincidence between the logic signals from these counters provided the trigger. The trajectories of individual beam particles could be reconstructed with the information provided by two small drift chambers (DC1, DC2) which were installed upstream of the trigger counters. This system made it possible to determine the location of the impact point of the beam particles at the calorimeter with a precision of typically ~0.2 mm. About 10 m downstream of the crystal, placed behind about 20 interaction lengths of material, a $50 \times 50\,\text{cm}^2$ scintillator paddle served as a muon counter. The first 10 interaction lengths consisted of the DREAM fiber calorimeter [7,8], which in this study only served to recognize and eliminate hadron contamination from the beam.

### 2.2. Data acquisition

Measurement of the time structure of the crystal signals formed a very important part of the tests described here. In order to limit distortion of this structure as much as possible, we used special 15 mm thick low-loss cables to transport the crystal signals to the counting room. Such cables were also used for the signals from the trigger counters, and these were routed such as to minimize delays in the DAQ system.[3] Other signals, e.g., from the muon counter and the calorimeter, were transported through RG-58 cables with (for timing purposes) appropriate lengths to the counting room. The crystal signals were sent into a unity-gain Linear Fan-out unit, output signals of which were used to measure the time structure and the total charge.

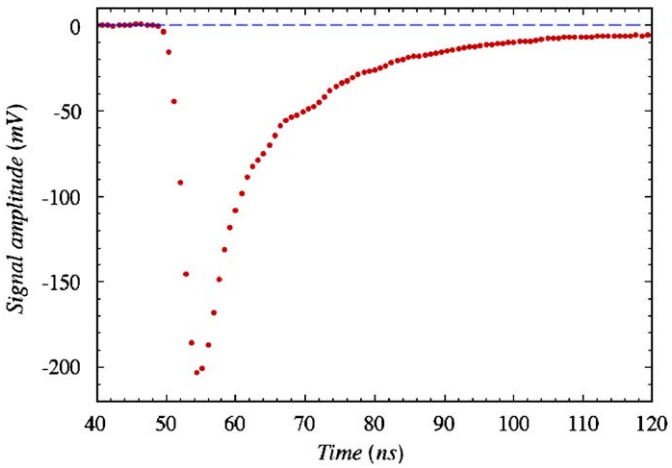


**Fig. 4.** Average time structure of the signals from 50 GeV electrons in the 1% Mo-doped $PbWO_4$ crystal, measured through the blue filter with $PMT_S$.

The data acquisition system used VME electronics. A single VME crate hosted all the needed readout and control boards. The charge measurements of the crystal signals were performed with a CAEN V792AC QADC module,[4] that offered 12-bit digitization at a sensitivity of 100 fC/count and a conversion time below 10 μs. The signals from the muon counters were integrated and digitized with a sensitivity of 100 fC/count, on a 12-bit LeCroy 1182 module.[5] The timing information of the tracking chambers was recorded with 1 ns resolution in a 16-bit 16-channel LeCroy 1176 TDC.[6]

The time structure of the calorimeter signals was recorded by means of a Tektronix TDS 7254B digital oscilloscope,[7] which provided a sampling capability of 5 GSample/s, at an analog bandwidth of 2.5 GHz, over four input channels. For the tests described in this paper, only two channels were sampled. The oscilloscope gain (scale) was tuned such as to optimize the exploitation of the 8-bit dynamic range, i.e., by choosing the sensitivity such that the overflow rate was ~1%.

The crystal signals were measured over a time interval during which time 282 data points were collected. The sampling rate depended on the type of crystal. For example, the signals from the Mo-doped $PbWO_4$ crystals were sampled every 0.8 ns, and the total interval thus lasted 224 ns. Because of the much longer decay time of the scintillation signals from the Pr-doped crystals, the sampling frequency was lower in this case: 2 ns per point (560 ns total interval length) or 4 ns per point (for a 1.12 μs interval). The time base of the oscilloscope was started by a trigger indicating the passage of a beam particle.

An example of the quality of the information obtained in this way is illustrated in Fig. 4, which shows the average time

[3] We measured the signal speed to be $0.78c$ in these cables.
[4] http://www.caen.it/nuclear/Printable/data_sheet.php?mod=V792&fam=vme&fun=qdc
[5] http://lecroy.com/lrs/dsheets/1182.htm
[6] http://www.lecroy.com/lrs/dsheets/1176.htm
[7] http://www.tek.com/site/ps/0,,55-13766-SPECS_EN,00.html

structure of the signals from 50 GeV electrons in the 1% Mo-doped crystal, measured through the blue filter with $PMT_S$.

Our readout scheme optimized the CPU utilization and the data taking efficiency thanks to the bunch structure of the SPS cycle, where beam particles were provided to our experiment during a spill of 9.6 s, with a repetition period of 48 s. During the spill, all events were sequentially recorded in the internal memory of the scope. We were able to reach, in spill, a data acquisition rate of ~2 kHz, limited by the size of the internal scope buffer. No zero suppression was implemented, so that the event size was constant: ~1.5 MB, largely dominated by the oscilloscope data.

### 2.3. Experimental data and analysis methods

The purpose of these tests was to split the crystal signals into their scintillation and Cherenkov components in the most efficient way. We exploited the following differences between these components to achieve this:

(1) Differences in *directionality*. Contrary to scintillation light, which is emitted isotropically, Cherenkov light is emitted at a characteristic angle by the relativistic (shower) particles that traverse the detector. We measured the signals for different orientations (i.e., angles $\theta$) of the crystal with respect to the beam.
(2) Differences in *time structure*. Cherenkov light is prompt, while the scintillation mechanism is characterized by one or several time constants, which determine the pulse shape. Detailed measurements of the time structure were performed (at different angles $\theta$) to study the properties of the prompt component in the signals from the crystals.
(3) Differences in the *spectral properties*. Cherenkov light exhibits a $\lambda^{-2}$ spectrum, while the scintillation spectrum is characteristic for the crystal in question (see Figs. 1 and 2). Of course, the extent to which these differences may be observed in the measured signals depends also on the filters and on the wavelength dependence of the quantum efficiency of the light detector ($PMT_S$, $PMT_R$).

The measurements were performed with 50 GeV $e^-$ beams. The angle $\theta$ between the crystal axis and the plane perpendicular to the beam line was varied between $-45^\circ$ and $45^\circ$, usually in steps of $5^\circ$. At each angle, 50 000 events were collected. In addition, 10 000 randomly triggered events provided pedestal information. For each event, the full time structure of the signals from the two PMTs reading the two sides of the crystal was recorded. In addition, ADC information from these channels was measured, as well as the ADC and TDC data from the auxiliary detectors (wire chambers, trigger counters, muon counters).

It is well known that the (scintillation) light yield of $PbWO_4$ crystals is strongly temperature dependent. In a previous study, we measured this effect to be $-2.6\%/^\circ C$ [4]. The temperature in the light-tight box housing the crystals was monitored with thermistors. The temperature variations were measured to be small in our setup, typically less than $\pm 2^\circ C$ over a 24-h cycle. No attempt was made to correct the signals for measured temperature variations. However, during each systematic study of a particular crystal, i.e., over a complete angular scan, or position scan, the temperature did not vary by more than $\pm 1^\circ C$.

Off-line, the beam chamber information could be used to select events that entered the crystal in a small (typically $10 \times 10\,mm^2$) region located around its geometric center. The electron beam contained a very small fraction (<1%) of muons and hadrons, which were eliminated with help of the downstream calorimeter and muon counter. Typically, more than half of the events survived these cuts.

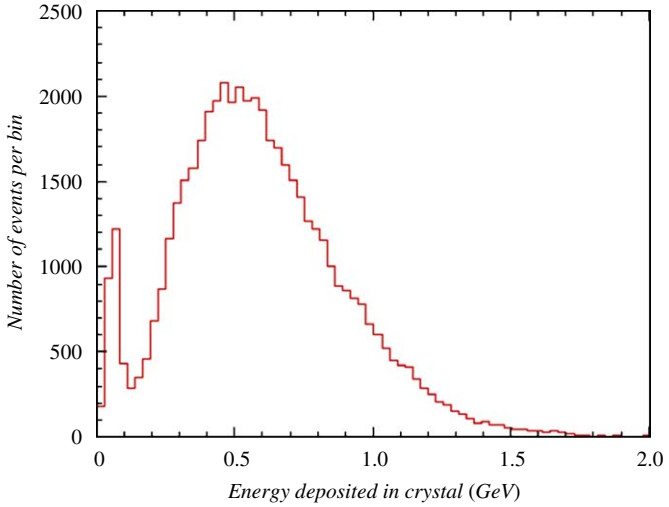


**Fig. 5.** Distribution of the energy deposited by 50 GeV electrons traversing the $PbWO_4$ crystal at $\theta = 30^\circ$.

An example of the time structure of the signals measured for electrons is given in Fig. 4. Fig. 5 shows a typical ADC signal distribution, measured by one of the two crystal PMTs. The energy scale in this figure was determined on the basis of a GEANT-4 simulation (see Section 3.4). A small (~2%) beam contamination of pions produced a mip signal in the crystal, which was well separated from the signals produced by the showering electrons, and easily recognized by the downstream calorimeter.

In order to determine the possible effects of instrumental factors on our results, we also performed a number of dedicated measurements. For example, in order to study the effects of light attenuation in the crystals, detailed scans (in steps of 1 cm) along the full length of the crystals were performed. In the case of the Pr-doped crystals, we also performed a series of measurements with different sampling rates and different filters.

### 2.4. Calibration of the detectors

The PMTs used in these measurements were calibrated with 50 GeV electron beams. The calibrations were carried out at $\theta = 0$, i.e., with the crystal oriented perpendicular to the beam line and the beam hitting the center of the crystal. In this geometry, 50 GeV electrons deposited, on average, ~355 MeV in the $PbWO_4$ crystals.[8] The absolute calibration of the signals generated by the crystal was not a major concern in these tests. The high voltages were chosen such that the average signals were about 300 ADC counts above the pedestal value. Off-line, the calibration constants of the ADCs (GeV/count) were fine-tuned such as to equalize the responses of the two PMTs, if needed.

For the time structure measurements, no separate calibration effort was performed. We only made sure that the vertical oscilloscope scale was chosen such that no pulse clipping occurred. As the crystals were rotated to larger angles $\theta$, the signals increased and the scale had to be adjusted, e.g., from 100 to 200 to 500 mV full range.

[8] This was determined with GEANT-4 Monte Carlo calculations. The energy scale of Fig. 5 was also determined on the basis of such calculations.

## 3. Experimental results for $PbWO_4$ : Mo

In this section, we mainly describe results obtained with the $PbWO_4$ crystal doped with 1% of molybdenum. At the end of the section, we describe effects observed as a result of increased doping levels.

### 3.1. Time structure of the signals

The molybdenum doping of the $PbWO_4$ crystals was intended to achieve two goals:

- a redshift of the scintillation spectrum, and
- an increase in the decay time of the scintillation signals.

The radioluminescence measurements (Fig. 1) suggest that essentially all light at wavelengths shorter than 400 nm should be the result of Cherenkov radiation in these crystals, while the wavelength region beyond 500 nm should be strongly dominated by scintillation light. This tendency was confirmed by our measurements of the time structure of the shower signals.

Fig. 6 shows the average time structure of the signals from the $PbWO_4$ crystal that was doped with 1% molybdenum. These signals were generated by 50 GeV electrons. The solid (blue) line represents the time structure measured on one side of the crystal, where a UV filter was mounted between the crystal and the PMT. The dotted (red) line represents the time structure measured on the other side of the crystal, where the light was filtered by the yellow filter. The photomultipliers used in these measurements were identical: $PMT_S$ on both sides. These two time structures, which were measured *for the same sample of events*, are spectacularly different. The UV light produced PMT signals that were very fast, >90% of the integrated signal was contained in a time interval of only 7 ns. The yellow light produced a signal with a rise time (10–90% of maximum amplitude) of 5 ns, and this signal decayed to 10% of its maximum value in 64 ns.

These characteristics strongly indicate that the light passing the UV filter produced an almost pure Cherenkov signal, while the light passing the yellow filter generated a signal that had all the characteristics of a scintillation signal. In Fig. 7, the latter signal is inverted and plotted on a logarithmic scale. The decay exhibits at least two different components. A fit by eye, represented by the two exponential curves, gives time constants of 26 and 59 ns, respectively, for these components.

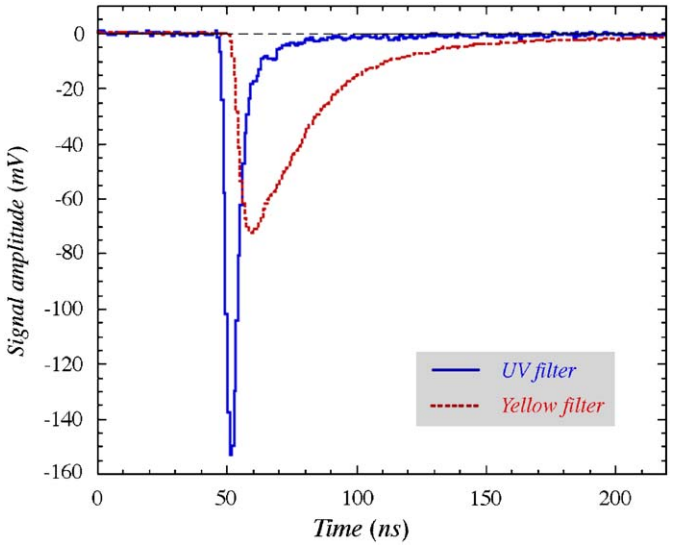


**Fig. 6.** Average time structure of the signals from a $PbWO_4$ crystal doped with 1% Mo, generated by 50 GeV electrons. The angle $\theta$ was 30° in these measurements. Shown are the results obtained with UV and yellow filters, respectively.

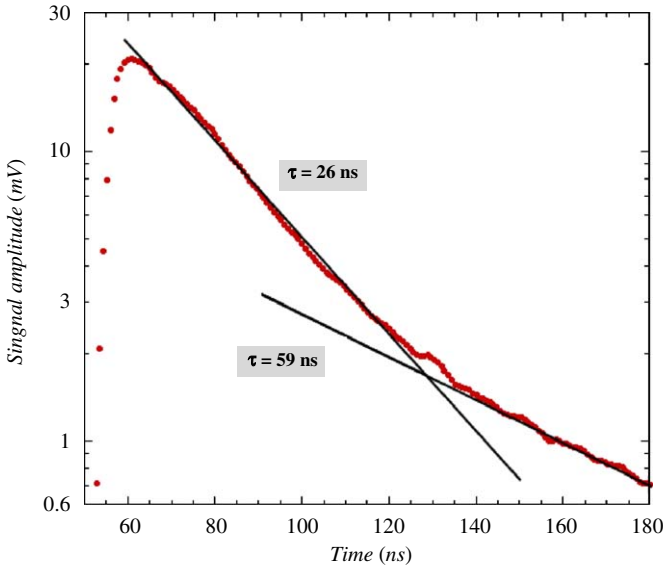


**Fig. 7.** Average time structure of the scintillation signal from the 1% Mo crystal, inverted and on a logarithmic scale. The straight lines, drawn to guide the eye, correspond to exponential decay times of 26 and 59 ns, respectively.

We repeated these measurements after replacing the UV filter by the blue one. As can be seen from Fig. 1, the effect of shifting the cutoff from 400 to 500 nm is that the blue light will contain a significant fraction of scintillation light, in addition to the Cherenkov light. This was confirmed by the measurement results, which are displayed in Fig. 8a. The time structure of the signal generated by the light transmitted by the yellow filter was not affected by this change, but the time structure of the signals produced by the blue light were significantly different from those from the UV light component (Fig. 6). The logarithmic representation of these results (Fig. 8b) shows that the tails of the time structures of the yellow and blue signals are essentially identical. It is interesting to note that the decay time of 26 ns is in excellent agreement with results reported by Nikl and coworkers [9], who characterized the properties of small samples of $PbWO_4$ crystals doped with various concentrations of molybdenum excited by radioluminescence, photoluminescence and thermoluminescence. For a concentration of 1%, they measured a decay time of 26.3 ns.

### 3.2. The Cherenkov/scintillation ratio

If the signals generated by the UV light indeed are completely dominated by Cherenkov radiation, as suggested by their time structure (Fig. 6), then their dependence on the angle of incidence of the beam particles ($\theta$, see Fig. 3) should be completely different from that for scintillation light.

Fig. 9 shows the ratio of the signals generated by the light transmitted by the UV and the yellow filters, as a function of the angle of incidence of the beam particles ($\theta$, see Fig. 3). The UV filter was mounted on the right-hand side ($R$) of the crystal, the yellow filter on the left-hand side ($L$) in these measurements, so that one would expect Cherenkov light to be mainly detected for positive values of the angle $\theta$, and most efficiently so when light emitted at the Cherenkov angle, $\theta_C = \arccos 1/n \approx 63^\circ$, impinges perpendicularly at the exit face of the crystal, i.e., at $\theta = 90^\circ - \theta_C \approx 27^\circ$. The distributions shown in Fig. 9 reach indeed their maximum value near that angle.

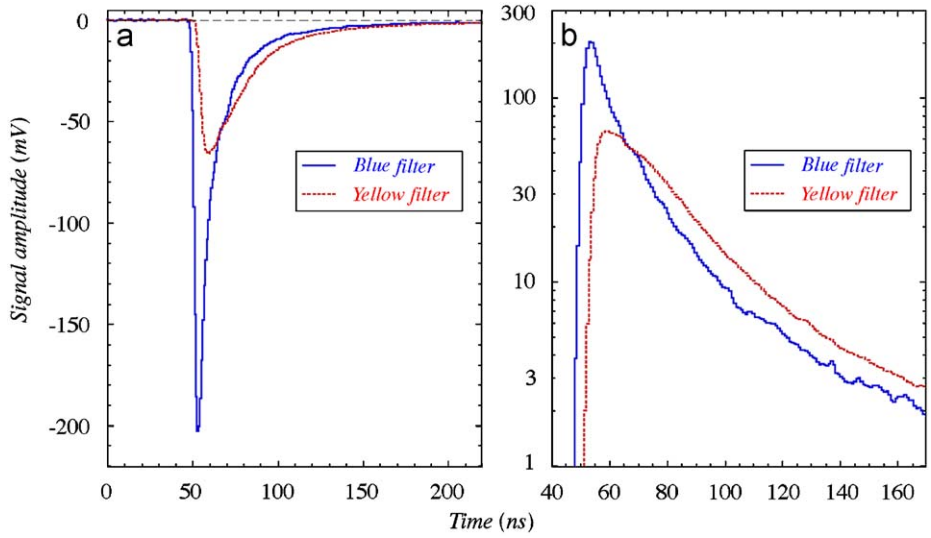


**Fig. 8.** Average time structure of the signals from a $PbWO_4$ crystal doped with 1% Mo, generated by 50 GeV electrons. The angle $\theta$ was 30° in these measurements. Shown are the results obtained with blue and yellow filters, respectively. The results are shown on linear (a) and inverted logarithmic (b) scales, respectively.

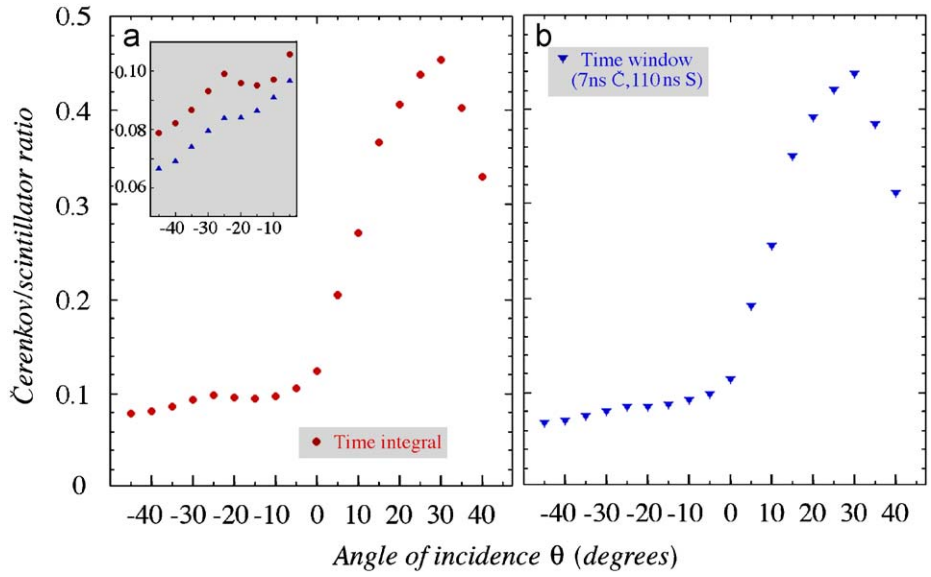


**Fig. 9.** Ratio of the signals from the light transmitted by the UV and the yellow filters, as a function of the angle of incidence of the beam particles (50 GeV $e^-$). The signals were obtained either by integrating over the entire time structure (a), or over limited time intervals chosen such as to purify their Cherenkov or scintillation content (b). The insert shows a blown-up version of the data at $\theta<0$.

The signals, and thus their ratio, were determined in two different ways for this analysis. In the first method, we simply integrated the signals over the entire time structure, i.e., over the entire 224 ns interval covered by the oscilloscope. These results are shown in Fig. 9a. In the second method, we attempted to optimize the Cherenkov content of the UV signals and the scintillation content of the signals from the light transmitted by the yellow filter. To that effect, the UV signals were integrated qover a 7 ns time interval ($t = 48-55$ ns), which contained >90% of the prompt peak seen in Fig. 6. The yellow signals were integrated over the time interval $t = 70-180$ ns. The ratio of the signals obtained in this way is displayed as a function of $\theta$ in Fig. 9b.

The first conclusion one can draw from a comparison of the distributions in Fig. 9a and b is that these are very similar. This means that there is no significant contamination of scintillation light in the signals produced by the light transmitted by the UV filter, since any such contamination would reduce the difference observed between positive and negative values of $\theta$. (Note that the distributions shown in Fig. 9 should be flat in $\theta$ if only scintillation light played a role.)

Upon closer inspection, one may notice a very small bump near the "anti-Cherenkov angle" ($\theta = -27°$), which is somewhat more pronounced in Fig. 9a. This is illustrated by the insert in Fig. 9a. This bump is the result of Cherenkov light that was reflected from the side where the yellow filter was mounted, and detected at the opposite side of the crystal. The efficiency for detecting such light is largest for $\theta = -27°$. However, since this light has to make a roundtrip in the crystal before being detected, it arrives somewhat later at the PMT than the direct Cherenkov light seen for $\theta>0$. Therefore, the effect is less pronounced in Fig. 9b, where a very narrow time interval was used to define the Cherenkov signals. The reflected light arrived too late in that case. Similar effects were observed in an earlier study [3].

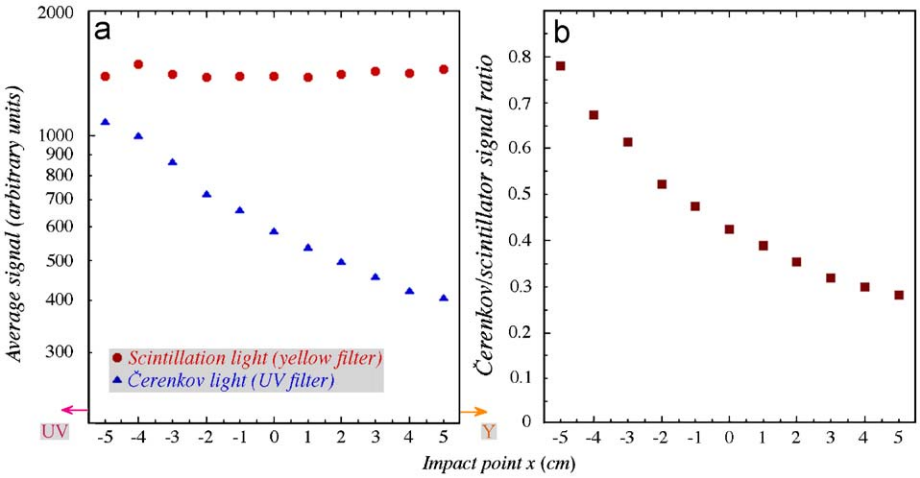


**Fig. 10.** Average signal from 50 GeV electrons in the $PbWO_4$ crystal doped with 1% Mo, as a function of the impact point of the particles. Shown are the signals generated by the light passing the UV and yellow filters, respectively, (a), and the ratio of these signals (b). The positions of these filters (UV,Y) are indicated.

### 3.3. Effects of light attenuation

Measurements in which the crystal was moved along the $x$-axis (see Fig. 3) made it possible to assess the effects of light attenuation on the signals. In these measurements, the crystal was oriented at an angle $\theta = 20^\circ$, in order to generate Cherenkov signals with a reasonable amplitude. The $L$ and $R$ sides of the 1% Mo-doped crystal were equipped with yellow and UV filters, respectively.

The results are shown in Fig. 10a, where the average signals observed in the PMTs on the two sides of the crystal are plotted as a function of the impact point of the 50 GeV beam electrons. While the signals generated by the PMT on the $L$ side, which measured the light transmitted by the yellow filter, were almost independent of the impact point, the signals generated by the PMT on the $R$ side (the UV-filtered light) decreased strongly as the distance to the point where the light was produced increased. Since these two PMTs measured almost pure scintillation and Cherenkov light, respectively, we conclude that the Cherenkov light was strongly attenuated in the crystal, whereas the scintillation light was not. Fig. 10b shows that, as a result of this difference, the Cherenkov/scintillation ratio varied by as much as a factor of three over a distance of only 10 cm. The attenuation length of the Cherenkov light amounted to ~10 cm.

### 3.4. The Cherenkov light yield

A limiting factor in the hadronic energy resolutions that can be obtained with dual-readout calorimeters is the Cherenkov light yield [1]. We have estimated the Cherenkov light yield of the Mo-doped $PbWO_4$ crystal using a method first described in Ref. [3]. The distribution of the scintillation signals produced by 50 GeV electrons traversing the crystal oriented at $\theta = 30^\circ$, and digitized with the ADCs, is shown in Fig. 5. We subdivided the horizontal scale of this distribution into 30 bins of equal width, and obtained the distribution of the (UV-filtered) Cherenkov signals for each of these bins, using the integral over the time structure measured with the oscilloscope. The fractional width ($\sigma_{rms}$/mean) of this distribution is shown as a function of the total signal in Fig. 11.

This signal (which was found to be approximately proportional to the deposited energy as derived from the yellow ADC signal) is plotted on a scale linear in its inverse square root, so that scaling

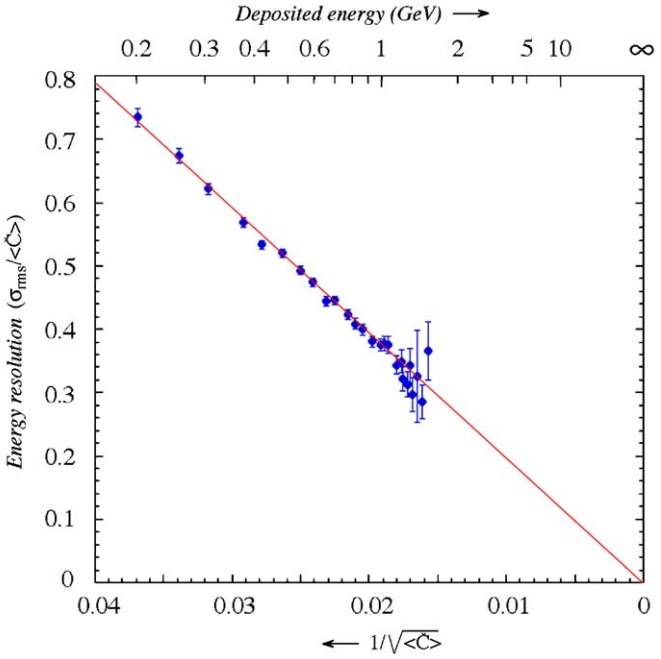


**Fig. 11.** The fractional width of the distribution of the Cherenkov signals from 50 GeV electrons traversing the $PbWO_4$ : Mo crystal, as a function of the total scintillation (yellow) signal measured with the ADC. The corresponding energy loss is indicated on the top axis. The crystal was oriented at $\theta = 30^\circ$.

with $E^{-1/2}$ implies the data points to be located on a straight line through the bottom right hand corner. The experimental data are indeed well described by such a straight line, any energy-independent deviations ("constant term") are statistically insignificant. The relationship between the signal units and the deposited energy was established with a GEANT-4 Monte Carlo simulation of the development of 50 GeV electron showers in a 2.0 cm thick $PbWO_4$ crystal oriented at an angle $\theta = 30^\circ$. This simulation showed that, on average, 0.578 GeV was deposited in this process. It allowed us to establish the relationship between the signals and the corresponding energy deposit, indicated by the horizontal scale on the top axis of the plot.

The energy dependence of the fractional width of the UV signals was found to scale with the inverse square root of the total

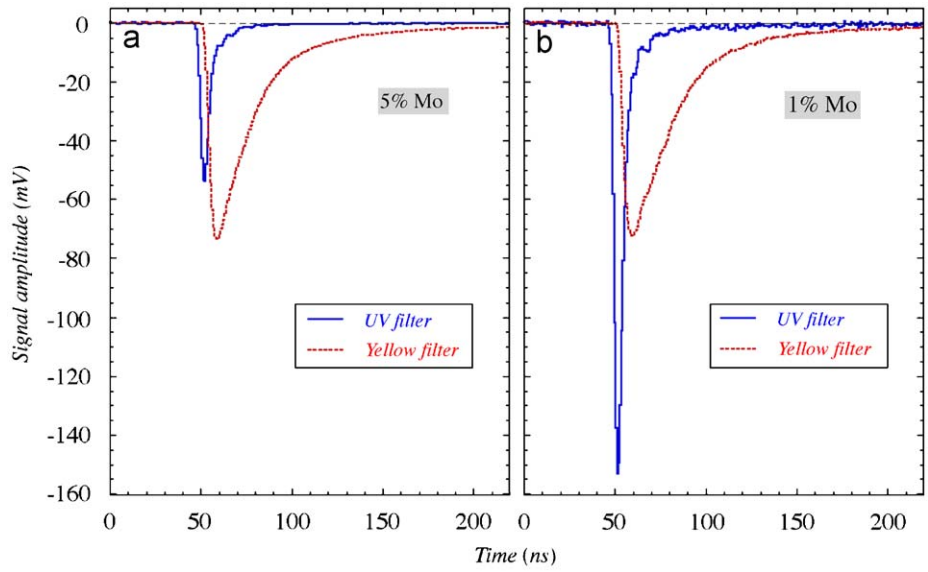


**Fig. 12.** Average time structure of the signals from a $PbWO_4$ crystal doped with 5% Mo (a) and 1% Mo (b), generated by 50 GeV electrons. The angle $\theta$ was 30° in these measurements. Shown are the results obtained with UV and yellow filters, respectively.

signal as

$$\frac{\sigma_{\rm rms}}{\langle \check{C} \rangle} = \frac{0.37}{\sqrt{E}} \quad (1)$$

with the energy $E$ given in GeV. This relationship is represented by the fitted curve in Fig. 11. We conclude from this that the number of Cherenkov photoelectrons per GeV deposited energy was about 8 (±1). The remarkably small value of this number is a consequence of the absorption characteristics of the UV filter and the strong attenuation of the light transmitted by this filter (see Fig. 10). This topic is further discussed in Section 4.5 where the light yield is compared with that from the Pr-doped crystals.

### 3.5. The 5%-Mo crystal

The $PbWO_4$ crystal doped with 5% molybdenum was tested much less extensively than the crystal that contained 5 times less of this impurity. The only data that make possible a comparison between these two crystals concerns measurements with 50 GeV electrons at angles of incidence $\theta = 0$, 30° and −30°, in which the filters, PMTs and high-voltage settings were the same, as in Fig. 6.

The average time structure of the signals measured on the two sides of the crystal, for an angle of $\theta = 30°$, is shown in Fig. 12a. As for the 1%-Mo crystal, the light transmitted through the UV filter seems to be pure Cherenkov radiation, while the light passing through the yellow filter appears to be completely dominated by scintillation processes. However, the ratio between these two signals is quite different from that in the 1%-Mo crystal, of which the results are shown in Fig. 12b. Whereas the scintillation signals are barely affected by the difference in the doping fraction, the signal produced by the light traversing the UV filter is smaller by about a factor of three. In Fig. 10, we saw that this light is already strongly attenuated in the 1% crystal. If the molybdenum is indeed responsible for this self-absorption, as suggested by [5], then an increase in the concentration is likely to further enhance this effect. This would provide a qualitative explanation of the observed phenomena.

Additional support for this explanation can be derived from Fig. 13b, in which the UV signals measured at $\theta = 30°$ are compared to those at $\theta = -30°$. The ratio between these two signals is about 30% larger than for the 1%-Mo crystal. As we saw in Fig. 9, the signals at $\theta = -30°$ contain a contribution from reflected light that has to travel 20 cm longer than the direct light in order to make a contribution to the signal. This component would completely disappear as a result of increased self-absorption.

While studying the differences between the signals observed at 30° and −30°, we also discovered another interesting phenomenon, illustrated in Fig. 13a. The time structures of the signals produced by light passing the *yellow* filter turned out to be different at these two angles. In particular, the time structure of the signal observed at $\theta = -30°$ contained a fast component which was absent at 30°. After subtracting the two time structures bin by bin, this fast component turned out to be identical in shape as the signals from the light passing the UV filter. Based on the observed characteristics, we concluded that this component was due to long-wavelength ($\lambda > 495$ nm, see Table 1) Cherenkov light. Since these signals were produced by a PMT with a multi-alkali (red-extended) photocathode, they contributed significantly to the overall signal from this side of the crystal. At $\theta = -30°$, Cherenkov light was found to constitute ∼8% of the total signal produced by the light traversing the yellow filter. A similar result was found in the signals from 1%-Mo crystal.

## 4. Experimental results for $PbWO_4$ : Pr

In this section, we describe the results obtained with the $PbWO_4$ crystals doped with praesodynium. In the first subsection, detailed results are given for the measurements performed on the crystal doped with 0.5% Pr with a specific set of filters. In subsequent subsections, we present the effects observed with different filters and different Pr concentrations. In Section 4.4, we investigate the effects of light attenuation on the Cherenkov light, which spoiled the performance of the Mo-doped crystals (Section 3.3) and in Section 4.5 the Cherenkov light yield is determined. All measurements on these crystals were carried out with the blue filter mounted on the right-hand side of the crystal ($PMT_R$, see Fig. 3). This side of the crystal, intended for detecting the Cherenkov component of the signals, was equipped with a regular PMT. The other side, intended for the detection of scintillation, was equipped with a red-extended PMT ($PMT_L$). The filter on this side was changed in order to optimize the

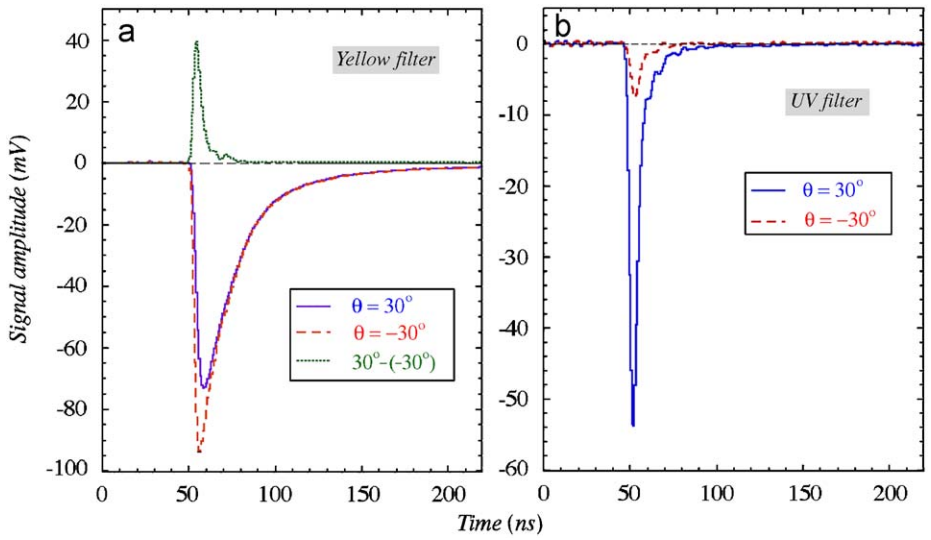


**Fig. 13.** Average time structure of the signals from a $PbWO_4$ crystal doped with 5% Mo, generated by 50 GeV electrons. Shown are the results obtained with yellow (a) and UV (b) filters, at angles $\theta = \pm 30^\circ$. In diagram (a), the difference between the time structures measured at these two angles is shown too.

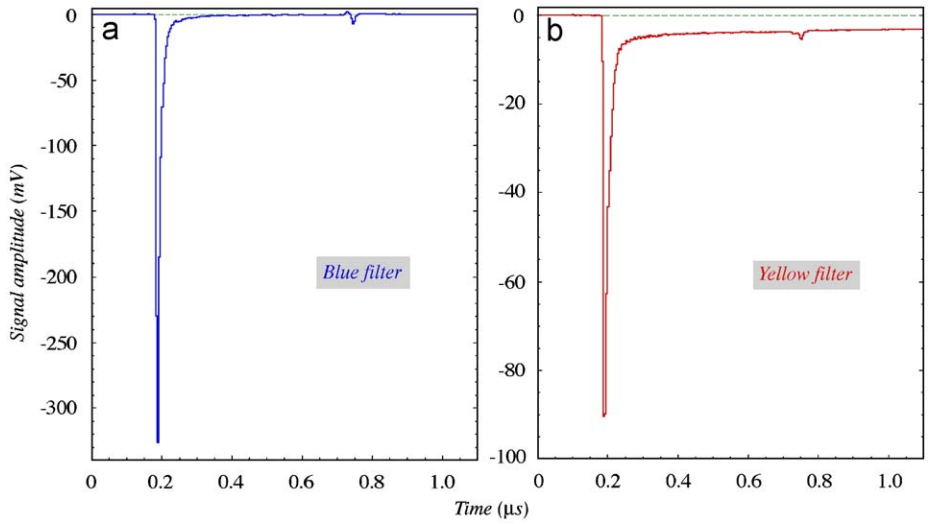


**Fig. 14.** Time structure of the signals from 50 GeV electrons in $PbWO_4$ crystal doped with 0.5% praesodynium, measured with light traversing the blue filter, in $PMT_R$ (a), and with light traversing the yellow filter (b), in $PMT_L$ (see Fig. 3). The crystal was oriented at an angle $\theta$ of 30°, and the signal amplitude was sampled at a rate of 4 ns/point.

sensitivity to the different components of the scintillation spectrum, indicated in Fig. 2. Two different sampling frequencies were used for these measurements: 0.4 ns/point, intended to study the Cherenkov component, and 4 ns/point, for the scintillation component of the light produced in these crystals.

### 4.1. The 0.5% Pr crystal: blue vs. yellow

All the results shown in this subsection concern measurements in which the left-hand side of the $PbWO_4$ : 0.5% Pr crystal was equipped with the "yellow" filter. As in all Pr measurements, the right-hand side was equipped with the "blue" filter (see Table 1 for the properties of these filters). The time structure of the signals generated by 50 GeV electrons in the PMTs detecting the filtered light is shown in Fig. 14.

The crystal was oriented at $\theta = 30^\circ$, such as to maximize the signal from the production of Cherenkov light. The signal from the blue side is shown in Fig. 14a, that from the yellow side in Fig. 14b. Interestingly, the latter signal also has a dominant prompt component, just like the blue signal, where we expect such a component as a result of the Cherenkov radiation.

In order to investigate the nature of this signal component, we studied its angular dependence. The signal amplitude was sampled at a rate of 0.4 ns/point for different angles of incidence of the 50 GeV electron beam. To that end, the angle $\theta$ was varied from $-35^\circ$ to $35^\circ$, in steps of $5^\circ$. Fig. 15 shows the time structures of the blue (diagram a) and yellow (diagram b) signals, measured at angles $\theta = 30^\circ$ (the solid histograms) and $-30^\circ$ (the dashed histograms), respectively. These results clearly indicate that the prompt component observed in the yellow signals is caused by Cherenkov radiation.

Additional evidence for this conclusion was obtained by studying the different angular characteristics of the "prompt" and "delayed" components of the signals from Fig. 15. These components were defined by integrating the signals over an interval of 7 ns around the peak (prompt) and from $t = 70-112$ ns (delayed), respectively. These results, shown in Fig. 16, may be

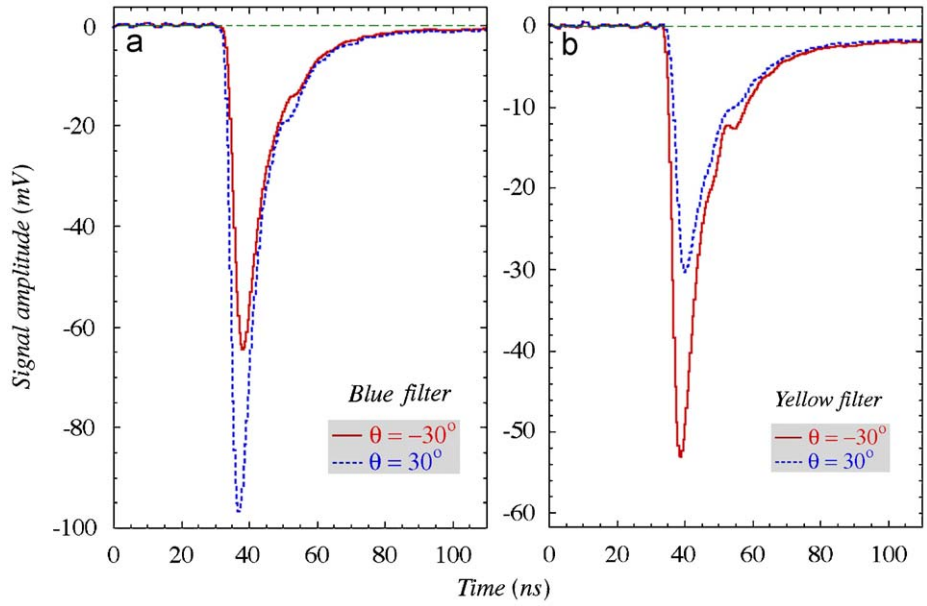


**Fig. 15.** Time structure of the signals from 50 GeV electrons in $PbWO_4$ crystal doped with 0.5% praesodynium, measured with light traversing the blue filter, in $PMT_R$ (a), and with light traversing the yellow filter (b), in $PMT_L$ (see Fig. 3). The crystal was oriented at an angle $\theta$ of 30° or −30°, and the signal amplitude was sampled at a rate of 0.4 ns/point.

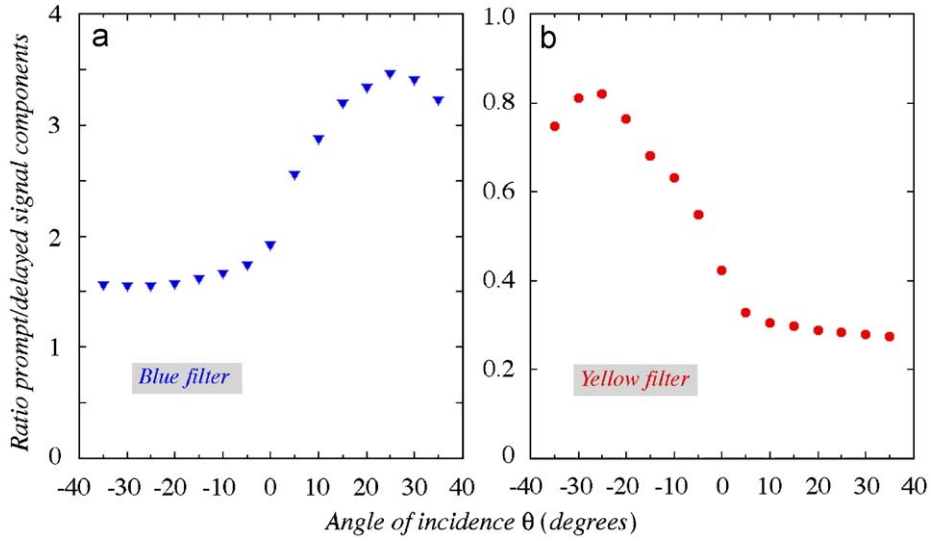


**Fig. 16.** Ratio of the prompt and delayed components of the signals from the light transmitted by the blue (a) or the yellow (b) filter, as a function of the angle of incidence of the beam particles (50 GeV $e^-$). The prompt component contained light detected during a time interval of 6 ns after the start of the signal, the delayed component was obtained by integrating from $t = 70-112$ ns (see Fig. 15).

compared with those from Fig. 9. The ratio of the prompt and delayed signal components reaches a maximum at $\theta = 30°$ for the blue light, just as in the comparable setup for the Mo-doped crystals. The fact that the prompt/delayed ratio reaches a maximum at $\theta = -30°$ for the yellow light confirms the Cherenkov nature of the prompt component in this case as well.

Apparently, the light transmitted by the yellow filter thus contains a very significant Cherenkov component, which is efficiently detected thanks to the use of a red-extended PMT. Part of the reason why this component is so prominently present in the time structure of the signal is the fact that the scintillation contribution to the signals is dominated by very slow components. This becomes apparent when we compare the time structures measured with the 4 ns/point sampling frequency (Fig. 14). Whereas the blue signal reaches the baseline shortly after the prompt peak (see also Fig. 15 for the high-sampling-frequency results), the yellow signal exhibits a long tail which has barely diminished when the sampling of the signal amplitude ends, 1100 ns after the trigger that started the time base of the oscilloscope.

The characteristics of this tail are shown in more detail in Fig. 17, where the signal amplitude is plotted as a function of time, from $t = 400-1100$ ns, i.e., starting about 200 ns after the prompt Cherenkov component (see Fig. 14b). Data are given for the three angles at which this measurement was performed ($\theta = 0, \pm 30°$).

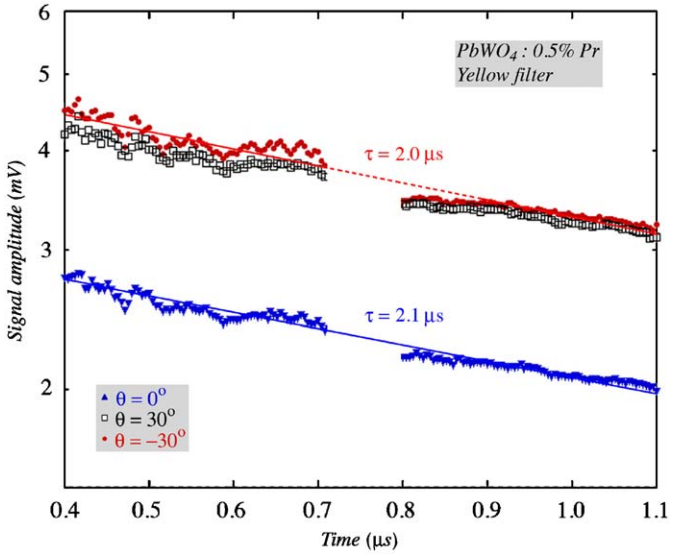


**Fig. 17.** Time structure of the tail of the signals observed from the $PbWO_4$ crystal doped with 0.5% praesodynium. The region where the reflection of the Cherenkov pulse was detected has been deleted for the sake of clarity. The results concern data where the 50 GeV electrons traversed the crystal at $\theta = 0^\circ$, $30^\circ$ and $-30^\circ$, respectively.

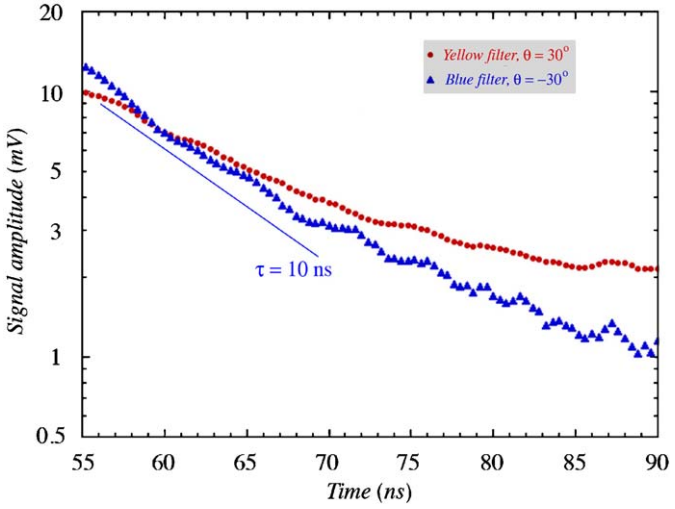


**Fig. 18.** Time structure of the signals $PbWO_4$ : 0.5% Pr crystal in the region immediately following the prompt Cherenkov peak, created by the light transmitted by the blue and the yellow filter. The angles $\theta$ were selected to minimize the contributions of eventual remnant Cherenkov contributions. The prompt component occurred at $t \approx 35$ ns on this time scale, which was defined by the start of the oscilloscope's time base by the trigger signal.

The smaller signal observed at $\theta = 0$ is just a consequence of the shorter path length of the particles in this case. For the sake of clarity, a small region between $t = 700$ and 800 ns has been deleted from this plot. Because of a small impedance mismatch at the end of the very long cables which transported the signals to the oscilloscope installed in the counting room, a reflection of the prompt signal component manifested itself in this part of the time structure, as can be seen in Fig. 14.

Fig. 17 illustrates that the long scintillation tail in the time structure of the signals is well described by an exponential decay with a time constant of about 2 μs. This is in good agreement with observations in which samples of this crystal material were studied with radioluminescence [6].

Earlier, we concluded from the angular dependence observed in Fig. 16 that the prompt peak observed in the yellow signal was caused by Cherenkov radiation. However, we can also conclude from the same figure that the delayed component in the blue signal indicates the presence of scintillation contributions. However, the fact that the baseline is almost restored within 50 ns after the prompt peak implies that this scintillation component is very short compared to the 2 μs characterizing the yellow tail. In Fig. 18, the signal portion immediately following the prompt peak is shown separately for the blue and yellow signals. In order to suppress eventual remnant contributions of Cherenkov light, we selected blue signals recorded at $\theta = -30^\circ$ and yellow signals at $\theta = 30^\circ$ for this purpose.

The figure shows indeed the presence of a short-lived scintillation component, in both signals. However, the decay constant of this component seems to be significantly shorter in the case of the blue light. For comparison, an exponential decay with a time constant of 10 ns is shown as well in this figure. This is the decay time of scintillation light produced in undoped $PbWO_4$ crystals [10]. This scintillation spectrum centers around 420 nm (see also Fig. 2) and is thus transmitted by the blue filter, which has a cut-off at 500 nm (Table 1). The time structure of the "yellow signal" in this region indicates a somewhat slower decay, since the long-wavelength remnants of undoped $PbWO_4$ scintillation light ($\lambda >$ 495 nm) are mixed with slower components resulting from Pr-induced wavelength shifting.

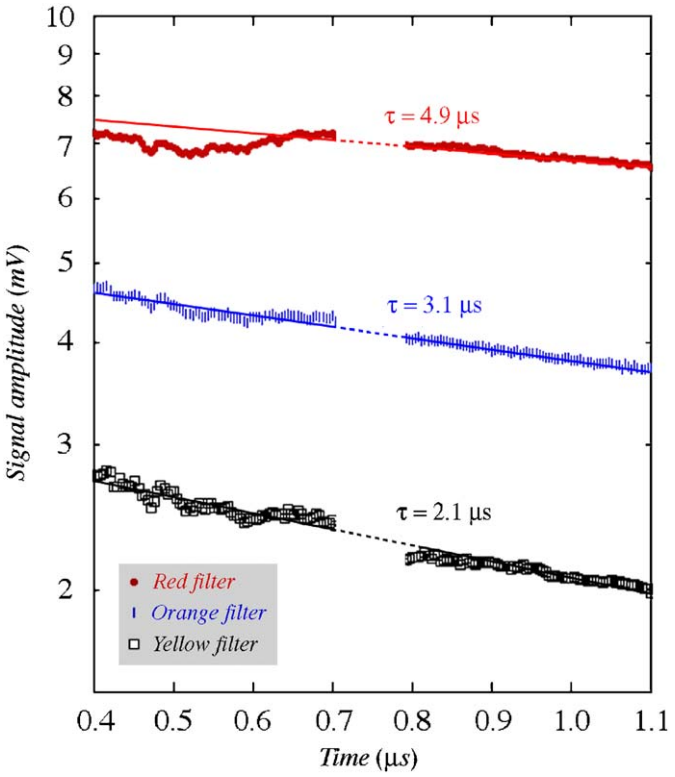


**Fig. 19.** Time structure of the tail of the signals observed in the $PbWO_4$ crystal doped with 0.5% praesodynium, measured with different filters. The region where the reflection of the Cherenkov pulse was detected has been deleted for the sake of clarity.

### 4.2. Changing the filter

All results shown so far concern the light that passed the yellow filter. In the following, we examine the effects of changing this filter by the "orange" or "red" one, or leaving it out altogether.

One clear effect of increasing the cut-off wavelength of the filter was a change in the decay constant of the slow scintillation

**Table 2**
Effects of the light filters on the decay characteristics and the relative abundance of scintillation light in the filtered signals from the $PbWO_4$ crystal doped with 0.5% praesodynium.

| Filter | Decay constant (μs) | $S/C$ ratio ($\theta = -30^\circ$) |
|---|---|---|
| GG495 (yellow) | $2.1 \pm 0.1$ | 1.38 |
| OG570 (orange) | $2.9 \pm 0.2$ | 2.06 |
| RG610 (red) | $5.1 \pm 0.5$ | 2.81 |

This abundance is defined as the ratio of the signals integrated from $t = 400-1100$ and 184–204 ns in Fig. 14a and its equivalent for the other filters, for the angle $\theta = -30^\circ$, at which detection of the Cherenkov component in the filtered light is maximized.

component of the signals. This is illustrated in Fig. 19, which shows the tail of the time structure of the signals produced by light traversing the yellow, orange and red filter, respectively. The exponential curves, drawn to guide the eye, show that the decay time increases from ~2 to ~5 μs when the cut-off wavelength is increased from 495 to 610 nm. This trend is consistent with observations made in radioluminescence experiments [6]. Nikl et al. reported lifetimes of 2–50 μs for the various components of the Pr light. Of course, in our setup, we did not measure the properties of these individual resonances separately, but integrated over the wavelength band transmitted by the filter and convoluted with the quantum efficiency curve of the PMT.

At the same time, the relative contribution of Cherenkov light to the signals from this filtered light was observed to *decrease*. This is illustrated in Table 2, which shows that the ratio of the signals integrated over the prompt peak and over the long tail (see Fig. 14) decreased by about a factor of two when the cut-off wavelength of the light was increased from 495 to 610 nm. Since the intensity of the Cherenkov radiation is proportional to $\lambda^{-2}$ while most of the scintillation light is concentrated in the wavelength region from 610 to 650 nm, this observation is not surprising.

### 4.3. Changing the doping concentration

We also studied $PbWO_4$ crystals doped with 1% or 1.5% praesodynium. In principle, one might expect three types of changes as a result of changing the doping concentration:

- a change in *light attenuation* as a result of increased self-absorption,
- a change in the *intensity of the scintillation* light, and/or
- a change in the *decay constants* of the scintillation process.

The first issue is addressed in Section 4.4, where we conclude that, unlike in the Mo-doped crystals, light attenuation did *not* affect the Cherenkov signals in these crystals. On the other hand, the total intensity of the scintillation light did increase with the concentration of praesodynium. Systematic studies which allowed us to quantify this statement were only carried out with the red filter. At $\theta = 30^\circ$, i.e., the angle at which contributions from Cherenkov light to the red signals were minimal, the total signal was observed to increase from a normalized value of 1.0 for the 0.5% crystal to 1.27 for the 1.0% crystal and 1.63 for the 1.5% crystal.

We also observed that the decay of the scintillation process became *faster* as the Pr-concentration was increased. As illustrated in Fig. 20, the tail of the time structure beyond the reflection of the prompt peak was well described by a single exponential. The time constant was observed to decrease from 4.9 μs for the 0.5% crystal to 3.9 μs for 1.0% crystal and 3.1 μs for the 1.5% crystal. Of course, we have to keep this in mind when interpreting the change in the

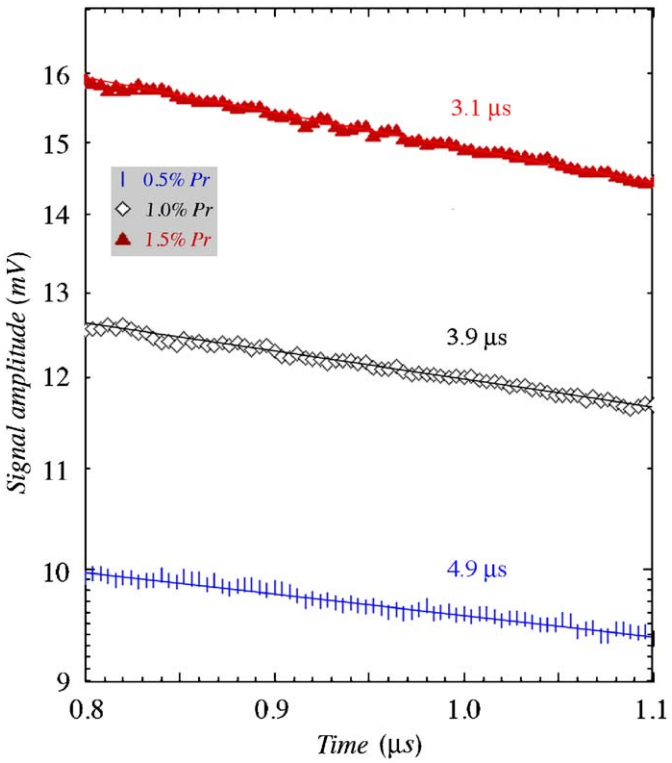


**Fig. 20.** Tail of the average time structure of the signals from 50 GeV electrons in the Pr-doped $PbWO_4$ crystals, oriented at $\theta = 30^\circ$. Shown are the results for three different doping concentrations. The results of exponential fits to the experimental are shown as well.

strength of the "red" signal mentioned above, since our measurements only concerned a period of about 1 μs after the start of the signal. It may thus well be that the increased signal strength was primarily a consequence of the faster decay. While the integrated signal was found to increase by 63%, the decay constant ($\tau^{-1}$) increased by 60% when the Pr-concentration was increased from 0.5% to 1.5%. Therefore, it seems that the main consequence of an increase in the Pr-concentration is a shortening of the time interval in which the scintillation light is released. This conclusion is commensurate with the findings of Nikl et al. [6].

### 4.4. Light attenuation

In Sections 3.3 and 3.5, we saw that light attenuation through self-absorption strongly affects the Cherenkov light produced in the Mo-doped $PbWO_4$ crystals. We studied the effects of light attenuation in the Pr-doped crystals in the same way, i.e., by means of a scan in which the electron beam entered the crystal at different points along its horizontal axis. The crystal was oriented at $\theta = 0$ in this scan, i.e., perpendicular to the beam.

Fig. 21a shows the average signals generated by 50 GeV electrons in the 0.5%-Pr crystal, as a function of the impact point of the particles. The circles represent the prompt component of the light that passed the blue filter, the triangles the integrated, unfiltered light measured on the other side of the crystal. The results are very different from those obtained with the Mo-doped crystals, the signals do not depend significantly on the distance the light had to travel to the PMT. In Fig. 21b, the ratio of both signals is plotted as a function of the impact point of the beam particles, for the 1.0% crystal. Interestingly, this result seems to exhibit an oscillating pattern. Similar patterns were observed in the position scan of the 0.5%-Pr crystal, and also in scans of a BGO crystal of which the results were reported earlier [3]. We attribute

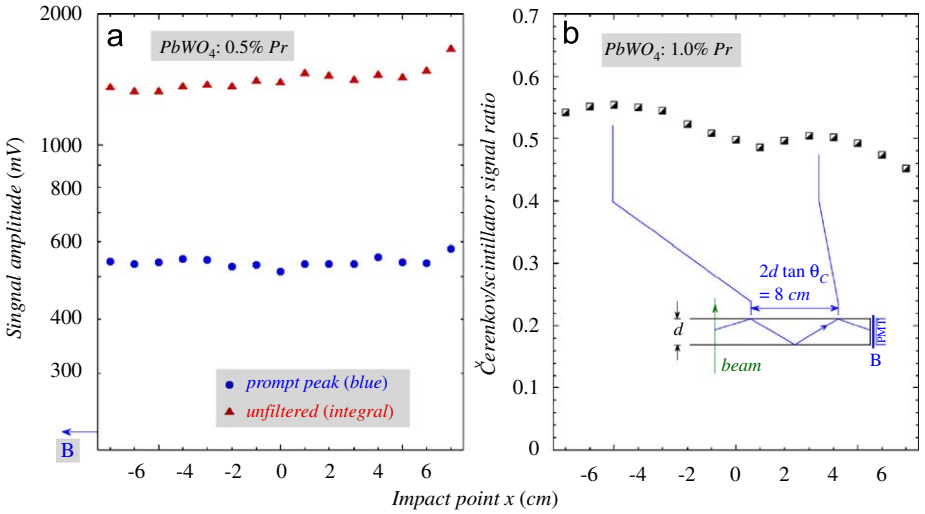


**Fig. 21.** Average signal from 50 GeV electrons in the $PbWO_4$ crystal doped with 0.5%Pr or 1.0% Pr, as a function of the impact point of the particles. Shown are the prompt signals generated by the light passing the blue filter and the integrated, unfiltered light for the 0.5% crystal (a), and the ratio of both signals for the 1% crystal. The position of the blue filter (b) is indicated. The insert shows the path of Cherenkov light on its way to the exit surface of the crystal.

this effect to a position dependence of the PMT that read out the blue light. The Cherenkov light generated by the beam particles represents a narrow cone which propagates through the crystal and illuminates the PMT in a non-uniform way. Non-uniformities in the quantum efficiency of the photocathode (which are very common near the edge) and/or in the optical contact between cookies, filter and PMT will thus translate into a position-dependent response to the Cherenkov signal. Any pattern in the Cherenkov response should repeat itself over a distance of $2d\tan\theta_C \approx 8$ cm, where $d$ is the thickness of the crystal and $\theta_C$ the Cherenkov angle (63°), as illustrated in the insert of Fig. 21b. Indeed, the response pattern exhibits this characteristic.

The differences in attenuation characteristics between the Mo- and the Pr-doped crystals can be understood from the differences in self-absorption of the light. Fig. 22 shows the absorption coefficient (i.e., the value of $k$ in $I(x) = I_0 e^{-kx}$) as a function of wavelength, for two different Pr-doped crystals (Fig. 22a) and the two Mo-doped crystals (Fig. 22b). The absorption coefficient for the undoped crystal is shown for reference purposes. The shaded areas represent the bandwidths of the light transmitted through the filters with which the measurements were performed, i.e., blue in the case of praesodynium, UV in the case of molybdenum. The cutoff at 310 nm was caused by the borosilicate PMT window. Fig. 22b shows that almost all the light from the Mo-doped crystals transmitted through the UV filter was very strongly attenuated. On the other hand, a large fraction of the light from the Pr-doped crystals transmitted through the blue optical filter, i.e., the light in the wavelength window 380–440 nm, was barely attenuated at all (Fig. 22a). The difference between the 1% and 5% molybdenum-doped crystals can also be understood from these absorption characteristics.

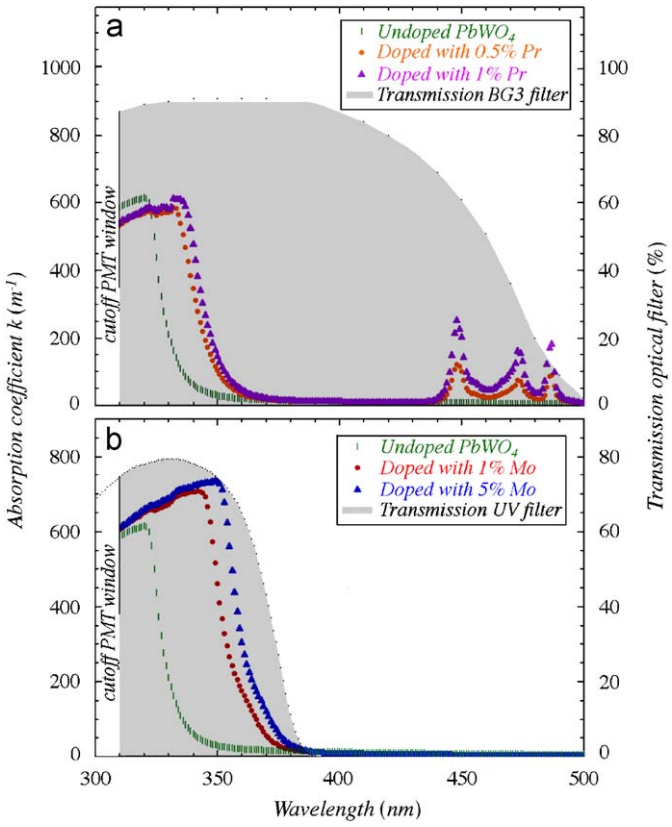


**Fig. 22.** The absorption coefficient as a function of wavelength, for two different Pr-doped $PbWO_4$ crystals (a) and for the two Mo-doped ones (b). Results for the undoped crystal are shown for reference purposes. The left-hand scale applies to all absorption coefficients. The shaded areas represent the bandwidths of the light transmitted through the optical filters with which the measurements were performed (right-hand scale).

### 4.5. The Cherenkov light yield

The Cherenkov light yield of the Pr-doped $PbWO_4$ crystals was measured in the same way as described in Section 3.4 for the Mo-doped ones. In this case, the light yield was found to be substantially larger.

This is illustrated in Fig. 23, which compares the distributions of Cherenkov signals measured in the two types of crystals, for 50 GeV electrons that deposited the same amount of energy, ~0.65 GeV, as measured by ADC that converted the (red) scintillation light detected by the PMT at the opposite side of the crystal. In the case of the Mo-doped crystal, the Cherenkov signal was obtained from the light traversing the UV filter, which contained almost no contamination of scintillation light (see Fig. 6). In the case of the Pr-doped crystal, the blue filter was used to obtain the Cherenkov signals. In order to eliminate

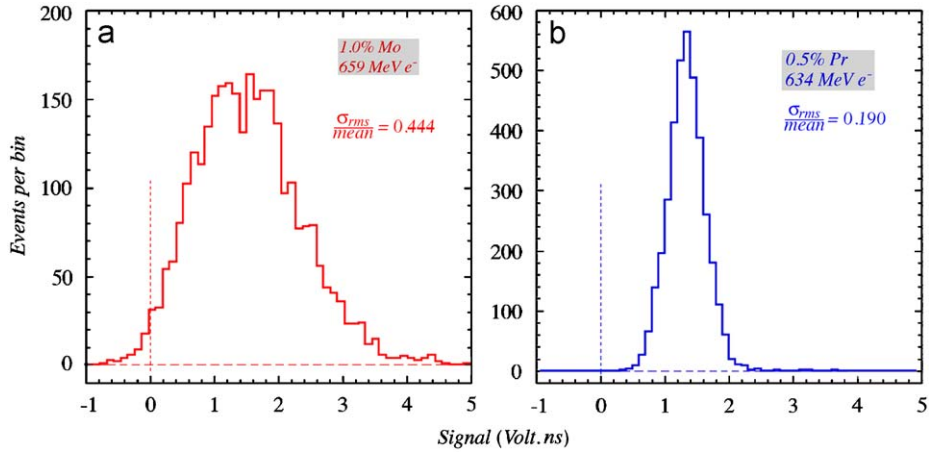


**Fig. 23.** Distributions of the Cherenkov signals from 50 GeV electrons traversing the $PbWO_4$ crystals doped with 1% Mo (a) or 0.5% Pr (b), when the beam particles deposited ~0.65 GeV in these crystals, as measured by ADCs that converted the red (scintillation) light generated in this process. The Cherenkov light was obtained with the UV filter in the case of the Mo-doped crystal, and with the blue filter in the case of the Pr-doped one. The crystals were oriented at $\theta = 30^\circ$.

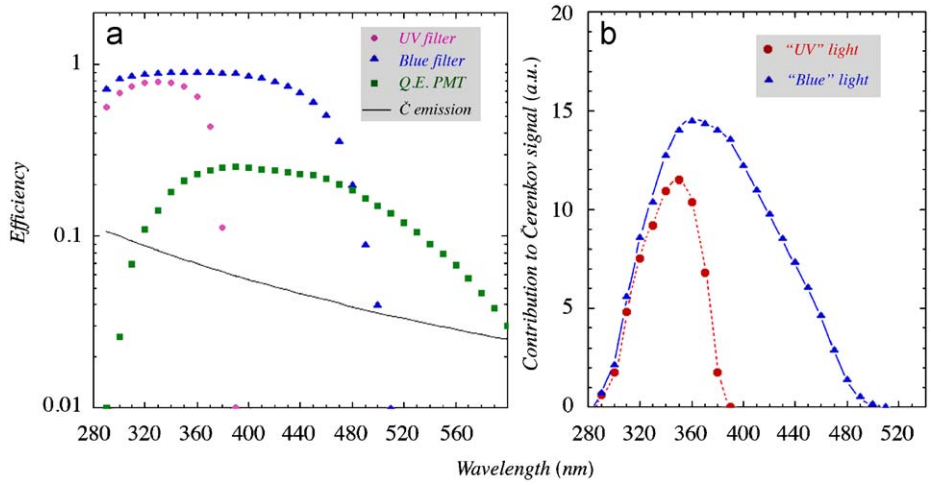


**Fig. 24.** The contribution of light of a given wavelengths to the Cherenkov signal is determined by the following factors: the transmission coefficient of the filter ("UV" or "blue") for light of that wavelength, the quantum efficiency of the PMT detecting the light passing this filter, and the intensity of the Cherenkov spectrum at this wavelength. This figure shows the wavelength dependence of these factors (a) and the resulting contribution to the Cherenkov signal when the UV or blue filter was used (b).

contaminating contributions from scintillation light (see Fig. 2), we only used the signal contained in the prompt peak (Fig. 14a) for this study.

The light yield follows directly from the relative width ($\sigma_{\rm rms}$/mean) of these distributions. In the case of the Mo-doped crystal, this width is 0.444, which corresponds to 5.1 photoelectrons, or 7.7 photoelectrons per GeV. In the Pr-doped crystal, the relative width amounts to 0.190, which represents the statistical fluctuations in 28 photoelectrons, or 44 photoelectrons per GeV deposited energy.

This large difference can be ascribed to two factors:

(1) The filters. The UV filter only transmitted light with $\lambda < 400$ nm, whereas the cutoff wavelength was 500 nm for the blue filter. Since the quantum efficiency of the PMT quickly decreased for $\lambda < 350$ nm, the detection window of the blue filter was significantly larger than that of the UV filter. Fig. 24 shows the implications of these effects quantitatively. The transmission coefficients of the UV and blue filters, the quantum efficiency of the PMT and the emission of Cherenkov light are plotted as a function of wavelength in Fig. 24a. The resulting contribution of light passing these filters to the Cherenkov signal is given in Fig. 24b. Integrated over all wavelengths, the Cherenkov signal is 2.7 times larger when the blue filter is used instead of the UV filter.

(2) The light transmitted through the UV filter in the Mo-doped crystal was attenuated by a factor of 2.5 in the 10 cm separating the production origin of the light and the PMT (Fig. 10). No such effect played a role in the case of the Pr-doped crystal (Figs. 21 and 22).

As a result of these two effects, we should thus expect the measured Cherenkov light yield to be about 6–7 times larger in the case of the Pr-doped crystal, in good agreement with the experimental observations.

## 5. Conclusions

We have investigated properties of $PbWO_4$ crystals doped with small amounts of molybdenum or praesodynium. This study was carried out to examine if such added impurities would improve

the suitability of $PbWO_4$ crystals for the purpose of dual-readout calorimetry. In evaluating the results, the following aspects are important:

- *Separability of the Cherenkov and scintillation signal components.* In undoped $PbWO_4$ crystals, it is very hard to obtain a reasonable separation, despite the fact that Cherenkov light constitutes a substantial fraction of the total light output (~15% [2]). The fast decay and the blue-dominated spectrum of the scintillation process are responsible for this. Attempts to use such undoped crystals as dual-readout calorimeters, using differences in the angular distribution [10] or the time structure of the signals [11] only yielded marginally useful results. Both the Mo- and Pr-doped crystals constitute a large improvement in this respect. We have found that simple light filters make it possible to obtain (almost) pure signals of either type (see, for example, Fig. 6). The contamination of scintillation light in the Cherenkov signals was at the sub-1% level, while contamination of Cherenkov light in the scintillation signals could be kept at the level of a few percent.
- *Time characteristics of the scintillation light.* Here, we observed a big difference between the two types of doping. In the Mo-doped crystals, components with decay times of 26 and 59 ns dominated (Fig. 7). This time scale is ideal for many calorimetric applications, and makes it much easier to separate the Cherenkov and scintillation signals on the basis of the time structure of the signals than for pure $PbWO_4$, where the decay time is 6–10 ns, depending on the temperature [4].On the other hand, the μs time scale of the scintillation signals in the Pr-doped crystals is clearly too long for applications in calorimetric detectors at high-energy particle colliders.
- *Self-absorption of the Cherenkov light.* In this respect, the measured characteristics of the Mo-doped crystals tested in this study make them impractical for calorimetric applications. Typically, hadronic showers fluctuate on a distance scale of 1 nuclear interaction length, which corresponds to ~20 cm in these crystals. Light attenuation lengths of the order of 10 cm, as observed in Fig. 10, are thus completely unacceptable in this context.
  On the other hand, self-absorption of Cherenkov light does not seem to be an important problem in the Pr-doped crystals.
  It is of course possible that the characteristics of the Mo-doped crystals could be improved for this application. The (effects of) attenuation of the Cherenkov light could be reduced by reducing the molybdenum concentration, which would shift the transmitted spectrum to shorter wavelengths. Replacing the transmission filter for the Cherenkov light with a band pass filter (eliminating the shortest wavelengths for which the attenuation is largest) could also be beneficial in that case (see Fig. 22).
- *Light yield of the Cherenkov signal.* The original DREAM calorimeter, which was based on optical fibers, had a Cherenkov light yield of 8 photoelectrons per GeV deposited energy [8]. This was a factor limiting its hadronic energy resolution, and one of the main reasons why we started looking into crystals as an alternative. The Cherenkov signals derived from the crystals tested in this study correspond to an effective light yield of ~8 photoelectrons per GeV in the case of the (1%) Mo-doped crystal and ~44 photoelectrons per GeV in the case of the (0.5%) Pr-doped one. The latter number would translate into a contribution of $0.15E^{-1/2}$ to the hadronic resolution, which would be non-dominant in practical devices. This light yield is thus adequate. The light yield of the Mo-doped crystal could possibly also be improved by using a lower doping concentration (which would reduce the self-absorption).

In summary, the tested crystals represent most definitely a considerable improvement with respect to undoped $PbWO_4$. However, in order to make them realistic candidates for application in practical calorimeters, further improvements would be needed. In particular, the scintillation process in the Pr-doped crystals is unacceptably slow and the self-absorption of Cherenkov light in the Mo-doped crystals is unacceptably large. Further studies to improve on these aspects are ongoing.

## Acknowledgments

We thank CERN for making particle beams of excellent quality available. We are also indebted to the *Radiation Instruments & New Components* company in Minsk (Belarus), which produced the crystals tested in this study in a timely manner and according to our specifications. This study was carried out with financial support of the United States Department of Energy, under contract DE-FG02-07ER41495, and by Italy's Istituto Nazionale di Fisica Nucleare.

## References

[1] R. Wigmans, New J. Phys. 10 (2008) 025003.
[2] N. Akchurin, et al., Nucl. Instr. and Meth. A 582 (2007) 474.
[3] N. Akchurin, et al., Nucl. Instr. and Meth. A 595 (2008) 359.
[4] N. Akchurin, et al., Nucl. Instr. and Meth. A 593 (2008) 530.
[5] M.V. Korzhik, et al., in: Proceedings of the IEEE Nuclear Science Symposium, Dresden, 2008.
[6] M. Nikl, et al., J. Appl. Phys. 104 (2008) 1.
[7] N. Akchurin, et al., Nucl. Instr. and Meth. A 536 (2005) 29.
[8] N. Akchurin, et al., Nucl. Instr. and Meth. A 537 (2005) 537.
[9] M. Nikl, et al., J. Appl. Phys. 91 (2002) 2791.
[10] N. Akchurin, et al., Nucl. Instr. and Meth. A 584 (2008) 273.
[11] N. Akchurin, et al., Nucl. Instr. and Meth. A 598 (2009) 710.